Thermodynamic and Dielectric Studies Concerning the Influence of Cylindrical Submicrometer Confinement on Heptyloxycyanobiphenyl

S. Diez,[†] D. O. López,*,†,‡ M. R. de la Fuente,‡ M. A. Pérez-Jubindo,‡ J. Salud,[†] and J. Ll. Tamarit[†]

Laboratori de Caracterització de Materials (LCM), Departament de Física i Enginyeria Nuclear, ETSEIB, Universitat Politècnica de Catalunya, Diagonal 647, 08028 Barcelona, Spain, and Departamento de Física Aplicada II, Facultad de Ciencia y Tecnología, Universidad del País Vasco, Apdo. 644, 48080 Bilbao, Spain

Received: July 26, 2005; In Final Form: October 14, 2005

Measurements of the specific heat and the static dielectric permittivity of heptyloxycyanobiphenyl (7OCB) confined to the 0.2 μm diameter parallel cylindrical pores of Anopore membranes in the isotropic phase and nematic mesophase, are presented. A comparison between the bulk and the confined 7OCB in treated and untreated pore wall surfaces using a chemical surfactant (HTBA) is performed. Both the treated and untreated membrane confinements seem to affect the nematic-to-isotropic phase transition by a downshift in transition temperature and some rounding at the specific-heat maximum, in a way similar to that which was earlier published for other liquid crystals confined in the same geometry. The static dielectric measurements clearly point out that untreated membrane confinement is axial, with the nematic director aligned parallel to the pore axis being homeotropic bulklike, i.e., with the nematic director aligned perpendicular to the electrode cell surfaces. After chemical surfactant treatment, the nematic director is constrained in a radial alignment being perpendicular to the pore walls. The dielectric measurements are revealed to be specially sensible to analyze the surface-induced nematic order due to the pore wall. The tricritical nature of the nematic-to-isotropic phase transition in bulk 7OCB as well as in treated and untreated Anopore confined geometries is discussed through both the specific heat and the static dielectric data.

1. Introduction

The confinement of liquid crystals to porous media provides a powerful tool to study of the effects of surface on the physical properties of liquid crystals that are susceptible of technological applications.[1–3]

The possibility of manipulate physical properties such as the diffusion constant or the refractive index of the porous media in which the liquid crystal is infiltrated by either varying temperature or applying an external field offers new insights in the technological applications of disordered and ordered porous materials.[3–7] Among possible applications, we find tunable photonic crystal lasers,[5] random lasers,[8–10] waveguides,[6] and optical limiters.[6]

Several types of porous materials can be used to confine liquid crystals. Among these, we can distinguish random porous networks as well as ordered porous materials. The former can be porous glasses with narrow pore size distributions but randomly oriented and interconnected pores (CPG, Vycor, etc.), Millipore filters made of a mixture of cellulose acetate and cellulose nitrate, aerogels in which the voids, highly irregular, are separated by randomly interconnected silica strands, and aerosil particles randomly dispersed in the liquid crystal. Ordered porous materials can be photonic crystals (two dimensional (2D) and three dimensional (3D)) in which the cavities maintain a strict periodicity in the plane (2D) or spatially (3D) or materials ordered in a lesser degree with nearly parallel cylindrical noninterconnected pores such as a 2D photonic crystal but without its periodicity in the distribution of pores. Examples of these last materials are: Nucleopore membranes made of polycarbonate films and Anopore membranes,[11,12] which will be extensively treated later.

Most of the work reported on confinement of liquid crystals in porous media has been devoted to phase transitions of alkylcyanobiphenyl liquid crystals (nCBs) confined in random porous network,[13–17] although in cylindrical geometries, mostly in Anopore membranes, some works[18–29] have been reported during the last decade of the 20th century and up to the present year. The amount of cited works seems to be considerable, although they are mostly focused to specific heat as well as deuteron nuclear magnetic resonance (DNMR) studies. Nevertheless, as for dielectric determinations in cylindrical geometry, the reported works are scarce[25–27] and likely the best studies were published during the last five years. Basically, these studies are devoted to the dynamic aspects rather than the static ones.

As a part of a more extensive study where dynamic properties are considered, the work dealt with in this paper is devoted only to the static properties (specific heat as well as dielectric static permittivity) of heptyloxycyanobiphenyl (7OCB) confined to 200 nm Anopore membranes. This compound is interesting because it displays only a nematic mesophase which exists over a wide temperature range with a first-order nematic (N)-to-isotropic (I) phase transition,[30] and finally, but not less important, it displays an adequate viscosity for confinement purposes. Likewise, the bibliographic data[18,19] of its homologous heptylcyanobiphenyl (7CB) also confined to 200 nm Anopore

* To whom correspondence should be addressed. Dr. David O. López Pérez, Departament de Física i Enginyeria Nuclear, ETSEIB, Universitat Politècnica de Catalunya, Diagonal 647, 08028 Barcelona, Spain. E-mail: david.orencio.lopez@upc.es.
† Universitat Politècnica de Catalunya.
‡ Universidad del País Vasco.

membranes would allow us to compare the effect of the oxygen atom in the terminal chain on the confining results. On the other hand, the static dielectric measurements on N mesophase, I phase, and through the N-to-I phase transition would allow a study to be done in a very precise way because of the induced orientational order due to the pore wall.

The thermodynamic study, through the specific-heat data, allows us to compare bulk and confined results for the N-to-I transition and from the calculated order parameter in the N and I phases. Compared to earlier publications on this field[18,19] in which only specific-heat data on several nCBs compounds (in particular 7CB) are reported, unpublished data on another nematic liquid crystal, 7OCB in this case, are provided.

The dielectric study was made in N mesophase as well as in I phase for both the bulk and confined cases, to get information about the order−disorder induced by the cylindrical confinement. In relation to earlier publications, as far as we know, only bulk 7OCB static dielectric data were reported.[31] Our static dielectric data for bulk were compared with those reported in the literature[31] as well as with data obtained for the confined configurations. An overall consistency on the information provided from the thermodynamic and dielectric studies is also discussed.

The paper is organized as follows. In section 2 we describe the experimental details. In section 3 a presentation of the specific heat as well as static dielectric results concerning the bulk 7OCB and confined configurations is done. In section 4, the discussion and data analysis are driven in three ways: first, the consistency of bulk results; second, the consistency of confined results, both through the specific-heat critical exponent and fluidlike model; third, an overall discussion. Finally, in section 5, a summary of the main conclusions is made.

2. Experimental Details

2.1. Materials and Sample Preparation. Liquid crystal 7OCB was synthesized and purified by Professor Dabrowsky in the Institute of Chemistry, Military University of Technology, Warsaw, Poland. The purity was stated to be higher than 99.9%, and no further purification was made.

Anopore membranes[11] consist of a high-purity Al_2O_3 matrix with diameter cylindrical pores from 200 nm down to 20 nm, being more or less parallel through their 60 μm thickness. Some properties such as their large porosity (more than 40%), high surface -to-volume ratio to maximize surface interaction, well-defined pore size, and adequate distribution of pores in the matrix constitute good elements for confined studies.

Anopore membranes (200 nm) were cut in disks of about 5 mm diameter. Each disk was cleaned in ethanol ultrasonic bath and dried by means of a thermogravimetry (TG) analysis up to 500 K in order to control and remove ethanol traces and impurities inside the pores. For confined liquid crystal molecular alignments, pore treatment was performed with a chemical surfactant (HTBA). To do so, each disk was immersed in a supersaturated solution of HTBA in *n*-hexane at about 343 K (boiling point) for a period of about a half an hour. When the disks were removed from the surfactant bath, a TG analysis at 343 K for a period of 10 min was performed to ensure the total solvent removal. Finally, treated and untreated membranes were immersed in an isotropic bath of 7OCB for a period of about 2 h. Filled membranes were carefully dried removing the excess liquid crystal material from the outer surfaces. Each single disk contained 0.8−0.9 mg of 7OCB which supposes an estimated average filling rate of about 85%, similar to that obtained for

us in a previous study for other liquid crystals in the same kind of confinement[28] and by other authors.[18,19]

2.2. Experimental Techniques. The experimental equipment used to perform the measurements have been the following: a TA Instruments DSC 2920 to obtain the specific-heat data by means of the modulated differential scanning calorimetry (MDSC) technique and a TA Instruments TG Q50 to perform the thermogravimetry (TG) analysis, an Olympus polarizing microscope equipped with a Linkam TMS-94 temperature controller, and finally, for the dielectric permittivity, an HP-4292A impedance analyzer was used on a plane capacitor. From all of this experimental equipment, two of them (thermogravimetry and the polarizing microscope) were only used in control tasks, while the other two deserve a special mention.
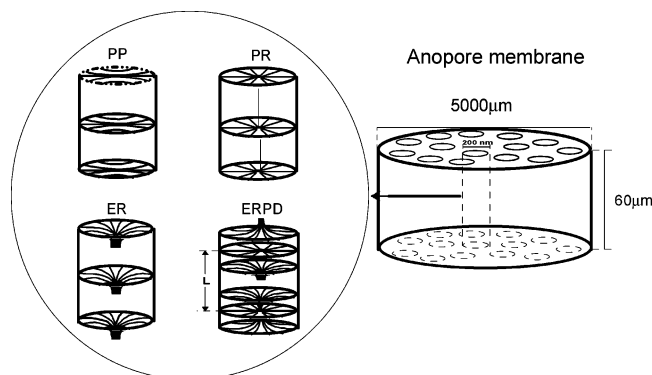
As for the specific heat measurements for which MDSC technique is used and for which extensive details can be found somewhere else,[32−34] it is important to realize that unlike an ac calorimeter, MDSC works in differential mode and, to do so, the specific heat of the membrane can be directly subtracted from the whole confined system (membrane + liquid crystal) by putting in the reference cell an empty membrane, exactly of the same characteristics as the filled membrane. Measurements were performed on cooling from the I phase down to the N mesophase and next on heating, both at 0.01 K·min^{-1}, with a modulation temperature amplitude of ±0.035 K and a period of 25 s.

As far as the static dielectric permittivity is concerned, a frequency of 10^5 Hz was chosen because it is lower than the relaxation frequencies of the molecular modes but high enough to avoid spurious effects related to the alumina, in such a way that this frequency could be assumed as the static permittivity. The plane capacitor (for the nonconfined samples) consisted of two gold-plated electrodes of 5 mm diameter separated by 50 μm thick silica spacers. For the confined samples, the capacitor was 60 μm thick. A modified HP16091A coaxial test fixture was used as the sample holder. It was held in a cryostat from Novocontrol, and both temperature and dielectric measurements were computer controlled.
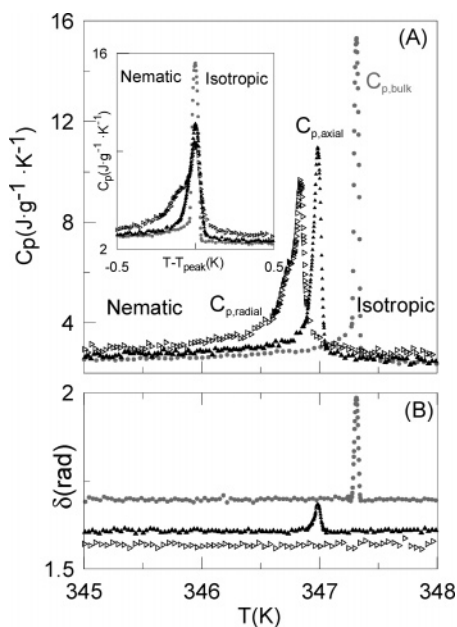
Dielectric relaxation studies in the range 10^6 to 1.8×10^9 were also performed using the Agilent 4291 A impedance analyzer. Although these studies will be published elsewhere, some results were used in order to rescale properly the permittivity of the confined liquid crystal. The measured capacity could be attributed to two parallel capacitors: the alumina matrix and the dispersed liquid crystal. In the studied frequency and temperature ranges, the permittivity of the alumina is nearly constant and then we can subtract the matrix capacity C_m from the measured capacity C_m: $C_{al} = (1 - p)C_0\epsilon_{al}$, where the average porosity of the membrane (p) is considered to be 0.7.[11] So, a temperature-dependent apparent complex permittivity for the liquid crystal ($\epsilon_{app} = (C_m - C_{al})/pC_0$), can be deduced. To compare the dielectric permittivities in the bulk and in confined geometries, the residual high-frequency permittivities in the isotropic phase can be compared by means of a rescaled factor R, defined as the ratio $\epsilon_{\infty,bulk}/\epsilon_{\infty,app}$, that depends on the molecular configuration. The data will be rescaled according to these values. Additional details on this technique can be found somewhere else.[28,34]

3. Results

3.1. Molecular Alignments of Confined 7OCB. The molecules of 7OCB confined to untreated Anopore membranes were homogeneously aligned more or less tangential to the pore cylindrical axis (axial alignment) as can be observed from

Heptyloxycyanobiphenyl Confinement in Cylindrical Pores

J. Phys. Chem. B, Vol. 109, No. 49, 2005 **23211**

Figure 1. Schematic representation of one Anopore disk along with some possible nematic director configurations in radial alignment: (PP) planar polar; (PR) planar radial; (ER) escaped radial; (ERPD) escaped radial with point defects.

Figure 2. Specific heat data (A) and δ phase shift (B) against temperature at the N-to-I phase transition for bulk and confined 7OCB. The inset shows these specific heat data as a function of $(T - T_{peak})$. All the data consigned have been obtained on heating. The δ data have been shifted in order to facilitate comparison.

TABLE 1: Thermal Properties of the N-to-I Transition for Bulk, Axial, and Radial 7OCB[a]

system	T_{NI} (K)	ΔT (K)	ΔH_{NI} (kJ·mol^{-1})
bulk[b]	347.31		0.33
axial confinement	346.98	−0.33	0.28
radial confinement	346.84	−0.47	0.29

[a] T_{NI} is the temperature at the specific heat maximum. ΔT is the shift from bulk. [b] A brief summary of the available thermal information on 7OCB from different bibliographic sources was made in ref 41.
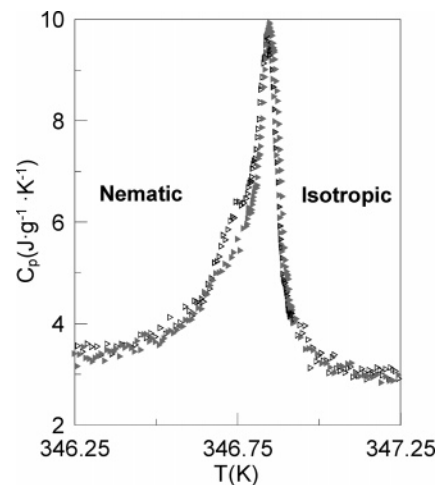
Figure 3. Detailed comparison of heating (horizontal triangles, open) and cooling (horizontal triangles, shaded) specific heat data near the N-to-I transition for the radial confinement.

sponding to bulk-7OCB (consigned in Table 1) are consistent with those already published by us[41] in which a brief summary of the available thermal information from bibliographic sources was made. As for both confinement configurations, specific-heat peaks clearly experiment downward shifts in temperature as well as a decrease of their apparent heights. Both effects are stronger for the radial case than for the axial one, being the later enhanced in the inset of Figure 2A. Transition temperatures T_{NI} corresponding to the apparent specific-heat maximum and temperature shifts ΔT_{NI} of the transition temperatures from the bulk are consigned in Table 1.

In Figure 2B, phase shift (δ) data through the N-to-I transition against temperature for bulk and confined samples are shown. Both bulk and axial confinement present a peak in δ, similar to that of the specific heat for the N-to-I transition. This feature in δ seems to be associated with the existence of latent heat at the transition and constitutes a signature of its weakly first-order character.[33] It is clearly observed that in the same way as for specific-heat data, the axial δ peak is broadened, downward shifted in temperature, and rounded extending more or less over the same temperature width. What it would seem surprising is the evolution of radial δ data through the transition. No changes of δ vs T are experimentally detected at the temperature corresponding to the maximum of the peak of the radial-specific heat data. In general this behavior is related to the lack of latent heat in the transition, and then it would be characteristic of a second-order transition. A known and old signature of the first-order character of a transition is the existence of thermal hysteresis, although it may be stressed that the absence of thermal hysteresis is not conclusive. In Figure 3, a comparison of the heating and cooling specific-heat data for the radial confinement is shown. It seems that despite the accuracy, no thermal hysteresis can be reported. Likewise, in such a figure, a small shoulder on heating run in the nematic side is clearly observed as in the inset of Figure 2A.

polarized optical microscopy (black texture in both isotropic and nematic phases). For HTBA-treated membranes, polarized optical observations show that axial alignment is lost in the nematic phase (yellow-gray texture). As published earlier for nCB liquid crystals,[18,35] the nematic molecular director seems to be more or less homeotropically aligned to the inner pore surface (radial alignment). Nevertheless, several radial configurations could be possible:[36−39] planar polar (PP), planar radial (PR), escaped radial (ER), and escaped radial with point defects (ERPD). A schematic representation is shown in Figure 1. Iannacchione et al.[19] considered ERPD as the most probable radial configuration for some nCB liquid crystals in Anopore membranes. Likewise, the same authors[40] from a numerical study pointed out the possibility of configurational transitions. So, the ER to PR transition would be discontinuous but involving small changes in energy making very difficult its experimental identification.
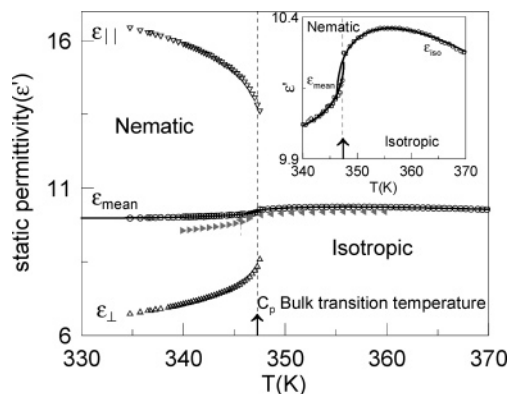
3.2. Specific Heat at the Nematic-to-Isotropic Transition. In Figure 2A, specific-heat data near the N-to-I transition against temperature for bulk and confined-7OCB in both axial and radial alignments are presented. First of all, the thermal data corre-

Figure 4. Static dielectric permittivity behavior in the isotropic and in the nematic phases of bulk 7OCB. The inset shows the behavior of the mean dielectric permittivity in the N mesophase and the dielectric permittivity in the I phase through the N-to-I transition. Solid lines are fitted by eqs 3a and 3b. Gray symbols are experimental data reported by Rzoska et al. in ref 31.

It should be noticed that the latent heat ΔH_{NI} associated with a first-order discontinuity in the enthalpy has been proved to be difficult to obtain with the required accuracy. Thus, for a given experiment, it is convenient to define

$$\Delta H_{NI}{}^{TOT} = \Delta H_{NI} + \int \Delta C_p \, dT \qquad (1)$$

where the last term of the right-hand side of eq 1 is the pretransitional fluctuation contribution (with ΔC_p being the excess specific heat, i.e., the difference between C_p and $C_{p,\text{background}}$) due to the change in ordering that is associated with the transition. If a phase transition is of second order, the latent heat ΔH_{NI} vanishes. The MDSC technique[33] enables us to determine in a direct manner both terms in eq 1. The estimated latent heats at the N-to-I transition (ΔH_{NI}) for bulk as well as axial- and radial-confined 7OCB are reported in Table 1.

3.3. Static Dielectric Permittivity of the Nematic and Isotropic Phases. In Figure 4, the bulk 7OCB static dielectric permittivity in the isotropic liquid and in the nematic mesophase is presented. The dielectric anisotropy is positive, and the parallel component of the static dielectric permittivity ($\epsilon_{\parallel}$) was easily obtained by applying a 40-V_{dc} voltage. The perpendicular component ($\epsilon_{\perp}$) was obtained using ITO/polyamide glass cells purchased from Linkam in which the surface effects were high enough to align the molecules parallel to the electrodes. The mean dielectric permittivity was calculated using the well-known expression: $\epsilon_{\text{mean}} = 1/3(\epsilon_{\parallel} + 2\epsilon_{\perp})$. At the inset of Figure 4, the isotropic and mean permittivity data in a zoom window around the N-to-I transition are shown in detail. Our bulk permittivity data are fully consistent in relation to the specific-heat transition temperature and slightly higher in relation to those reported by Rzoska et al.[31] which are shown in Figure 4 (gray horizontal triangles).

In Figure 5, the apparent static dielectric permittivity data for confined 7OCB in both axial (ϵ_{axial}) and radial (ϵ_{radial}) alignments, rescaled by applying the corresponding R factors ($R_{\text{axial}} = 1.73$; $R_{\text{radial}} = 1.86$), are shown. Owing to our experimental setup, ϵ_{axial} and ϵ_{radial} account for the components in which the molecules are aligned parallel and perpendicular to the electric field, respectively. From an overall inspection of Figure 5, no difference in transition temperature seems to exist between both sets of confined results. This fact is clearly shown at the inset of Figure 5 in which a 10 K zoom around the N-to-I transition is presented. Absolute apparent static dielectric values in relation to the bulk values should be considered with caution
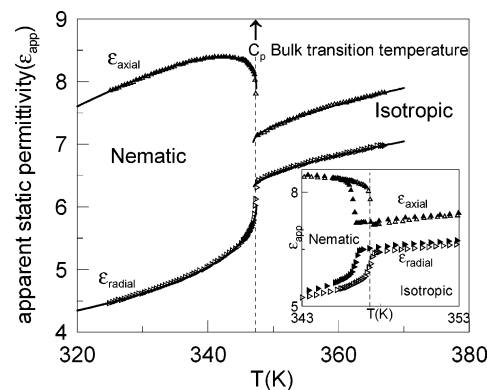
Figure 5. Apparent static dielectric permittivity behavior in the I and the N phases of 7OCB in both the axial and radial confinements. The inset shows the behavior of these apparent dielectric permittivities on heating (open triangles) and on cooling (shaded triangles) in the N mesophase and in the I phase through the N-to-I transition. Solid lines are fits through eqs 6a and 6b.

as already mentioned in section 2. Cooling data for confined samples are also displayed pointing out the existence of a considerable thermal hysteresis (about 1 K) for both confinement configurations.

4. Data Analysis and Discussion

4.1. Consistency of 7OCB Bulk Data Analysis. As mentioned earlier, bulk 7OCB displays only a nematic (N) mesophase that experiments a phase transition to an isotropic (I) phase known to be first order as a result of symmetry requirements.[30] Nevertheless, its critical behavior at the transition could be analyzed through very precise experimental data of certain physical magnitudes such as, for instance, specific heat or static dielectric permittivity. If specific heat is taken into account, the data could be analyzed using the standard expressions[19,42] for N and I phases excluding all the points in the N−I coexistence region

$$C_p{}^N = B + D\left[\frac{T}{T^{**}} - 1\right] + A_N\left|\frac{T}{T^{**}} - 1\right|^{-\alpha} \qquad (2a)$$

$$C_p{}^I = B + D\left[\frac{T}{T^*} - 1\right] + A_I\left|\frac{T}{T^*} - 1\right|^{-\alpha} \qquad (2b)$$

where T^{**} denotes the temperature at which the N-to-I transition would occur coming from the N phase if it were second order and T^* has the same meaning when temperature decreases from the I phase. Both temperatures must verify that T^{**} is higher than T^*. In the limit when the transition is of second order, both temperatures are set equal. The corresponding amplitudes above and below the transition are A_I and A_N, respectively, whereas B and D account for the specific heat background, both being above and below the transition. The specific-heat critical exponent is α, also the same above and below the transition, in such a way that it should be 0.5, as predicted either by extended Landau−de Gennes mean-field theory or by the tricritical behavior.[42,43]

In Figure 6, the 7OCB bulk C_p and δ phase shift data are shown again. The later were used to identify, by a sharp change, the excluded points of the coexistence N−I region (shaded area in Figure 6). A range of data spanning approximately 2 K was chosen in the N mesophase below the coexistence region for which eq 2a was used to do a preliminary fit of five parameters (α, B, D, A_N, and T^{**}). In the same way, in the I phase above the coexistence region, a second set of points spanning ap-

TABLE 2: Results of Fits to Equations 2, 3, and 5 for Bulk and Axial 7OCB[a]

physical magnitude	N	a	A_N/A_I	T^* (K)	T^{**} (K)	$10^3\chi^2$
			Bulk			
specific heat	200 (N)−150 (I)	0.508 ± 0.002	3.91 ± 0.67	347.29 ± 0.40	347.34 ± 0.20	2
dielectric constant	50 (N)−150 (I)	0.50 ± 0.05	−0.70 ± 0.29	346.28 ± 0.10	347.52 ± 0.70	1
			Axial Confinement			
specific heat	300 (N)−200 (I)	0.50 ± 0.05	3.17 ± 1.23	346.97 ± 0.90	346.99 ± 0.1	4
dielectric constant	230 (N)[b]	0.54 ± 0.02	3.58 ± 0.8	346.94 ± 0.80[c]	347.41±0.15	0.3
	150 (I)[b]	0.50 ± 0.01				0.2
			Radial Confinement			
specific heat	300 (N)−200 (I)	0.52 ± 0.04	1.94 ± 1.31	346.78[d]	346.85 ± 0.05	50
dielectric constant	235 (N)[b]	0.54 ± 0.03			347.42 ± 0.13	0.2
	150 (I)[b]	0.50 ± 0.01	3.68 ± 0.9	346.94 ± 0.80[c]		0.2

[a] N is the number of data points included in these fits. The errors quoted are the statistic uncertainties. [b] Both fittings were performed in an independent way, without imposing the same α value for both N and I phases. [c] Both temperatures were fitted in an independent way. [d] This value was held fixed in order to fit the same α value for both N and I phases.
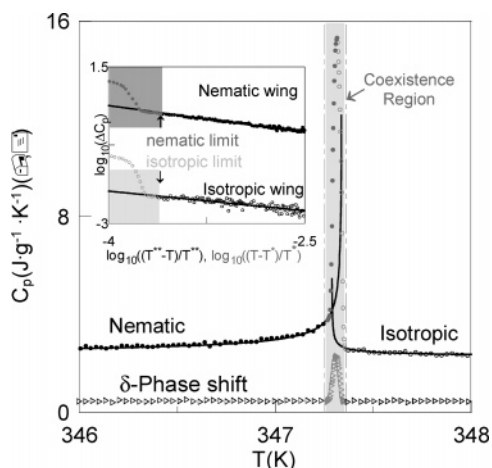
Figure 6. Specific heat (●, ○) against temperature near the N-to-I transition for bulk-7OCB. δ phase shift data (horizontal triangles, open) are included to delimit the coexistence region (shaded area). The inset shows in a double logarithmic plot ΔC_p ($C_p − C_{p,\text{background}}$) vs reduced temperatures.

proximately 1 K was considered in eq 2b to fit also five parameters (α, B, D, A_I, and T^*). Common parameters in both phases (α, B, D) were simultaneously refined and then the final A_N, T^{**}, A_I, and T^* were obtained. All the parameters are collected in Table 2 and represent well enough the measured specific heat data, as indicated by χ^2 values and as seen in Figure 6 in which both equations (2) are drawn. In the inset of Figure 6, in a double logarithmic plot, a linear relationship, with slope $-\alpha$, is found between ΔC_p ($C_p − C_{p,\text{background}}$) and reduced temperatures (($(T^{**} − T)/T^{**}$ or $(T − T^*)/T^*$) for both nematic and isotropic wings. It may be underlined the symmetry of the coexistence region.

If the static dielectric permittivity data are taken into account, the behavior shown in Figure 4 could be analyzed through the fluidlike model.[31,44,45] In such a model, the isotropic and mean permittivity data can be fitted by

$$\epsilon_{\text{iso}} = \epsilon^* + a_I|T − T^*| + A_I^D|T − T^*|^{1-\alpha} \quad (3a)$$

$$\epsilon_{\text{mean}} = \epsilon^{**} + a_N|T − T^{**}| + A_N^D|T − T^{**}|^{1-\alpha} \quad (3b)$$

where α, T^*, and T^{**} have the same meaning as in eq 2. The A_I^D and A_N^D are the corresponding dielectric amplitudes that should be equivalent to those reported in eq 2 for the specific heat. The latter was predicted by Mistura[46] in 1974 for the anomaly of dielectric permittivity in homogeneous critical mixtures and much more recently Rzoska et al.[31] suggested that

the derivative of the dielectric constant with temperature should be proportional to the specific heat. So, from fluidlike relations (eqs 3), $A_I^D(1 − \alpha)$ and $−A_N^D(1 − \alpha)$ should be proportional to the specific heat amplitudes A_I and A_N, respectively, in such a way that the ratio between both amplitudes should be virtually the same. By means of eq 3, five parameters have been fitted for each phase, being the more representative α, the amplitude ratios, and temperatures T^* and T^{**}, all consigned in Table 2. All these parameters represent well enough the measured isotropic and mean permittivity data, as indicated by χ^2 values and as seen in Figure 4 and in the inset of this figure in which both equations (3) are drawn.

From Table 2, although the critical exponent α is about 0.5 whatever the data (specific heat or dielectric) are considered, there are some differences when dielectric parameters are compared with those obtained from specific heat. Probably, the most relevant is addressed to T^* for which the difference is about 1 K. Likewise, the difference between T^{**} and T^* is more than 1 K from dielectric data, comparable to that obtained by Rzoska et al. for the same compound. Nevertheless from specific-heat data, this difference is much smaller (≈0.05 K). This fact was already cited by Anisimov,[42] which discussed the N-to-I phase transition in bulk liquid crystals in the 1980s. Another aspect to which attention must be paid is the ratio of amplitudes (A_N/A_I) that from specific-heat data is 3.91, a value similar to that reported by Iannacchione et al.[19] for some nCB compounds. With dielectric data of about −0.7, a value that if we take the derivatives of eq 3, transform into a positive value that is still far away from 3.91. Even so, both values are much lower than those found for the tricritical behavior of ^{3}He + ^{4}He for which the amplitude ratio is about 7.[47] Tricritical amplitude ratios of about 1.6 were experimentally found in the past[33,48−50] for the smectic A-to-N transition in which a negligible latent heat was reported. Values about 3 were also reported for the N-to-I transition.[51] Keyes[52] suggested that tricritical exponents should be expected rather than those predicted by Landau−de Gennes mean-field theory. In fact the nematic order parameter exponent (β) in several systems seems to be consistent with the tricritical value ($\beta = 1/4$). In our case, the average nematic order parameter in the bulk (S_N) can be obtained through either the dielectric anisotropy $\Delta\epsilon = \epsilon_{||} − \epsilon_{\perp}$ ($S_N \propto \Delta\epsilon$) or from specific-heat data following the procedure of Iannacchione et al.[19] in which

$$S_N^2 = \frac{2M}{aV}\left[\int_{T_{EN}}^T \frac{\Delta C_p}{T}\, dT + \frac{\Delta H_{NI}}{T_{NI}} + \int_{T_0}^{T_{EI}} \frac{\Delta C_p}{T}\, dT\right] \quad (4)$$

where M and V are the mass and volume of the system,
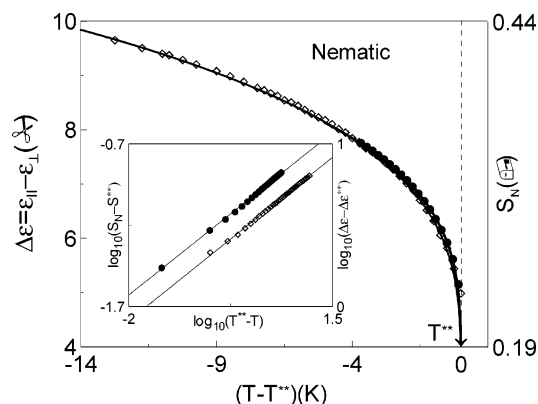
Figure 7. Measured dielectric anisotropy $\Delta\epsilon$ ($\diamond$) and calculated average nematic order parameter S_N ($\bullet$) against their respective ($T - T^{**}$). The inset shows a double logarithmic plot ($S_N - S_N^{**}$) and ($\Delta\epsilon - \Delta\epsilon^{**}$) vs reduced temperatures, according to eq 5.

respectively, and a is the first coefficient in the Landau–de Gennes free energy density expansion ($f = f_0 + \frac{1}{2}a(T - T^*)S^2 + ...$; assuming the other coefficients of the expansion are temperature independent). The value of a is taken as 0.13 $J\cdot K^{-1}\cdot cm^{-3}$ (the standard value for the pentylcyanobiphenyl 5CB, assuming that this value for 7OCB could be comparable). The integration must be numerically done, from T_0 in the I phase, well above T_{NI}, at which the order parameter could be considered zero down to T in the N mesophase. T_{EI} and T_{EN} are the limit temperatures of the coexistence region in the isotropic and nematic phases, respectively.

In Figure 7, the thermodynamic order parameter (eq 4) along with the dielectric anisotropy $\Delta\epsilon$ against $T - T^{**}$ are shown. To parametrize both sets of experimental data the expression

$$S_N = S^{**} + B|T - T^{**}|^{\beta} \qquad (5)$$

can be used, in which T^{**} values have the same meaning as in eqs 2 and 3. Really, for us, the most interesting parameter in eq 5 is the exponent β which is found to be 0.29 (± 0.05) irrespective the dielectric anisotropy data or S_N data are considered (see inset of Figure 7), being this value very close to the tricritical behavior.

4.2. Consistency of 7OCB-Confined Data Analysis. The tricritical behavior of both axial and radial confined configurations has been also analyzed using specific-heat and dielectric data, following a similar procedure to what has been exposed in the previous section devoted to the bulk-7OCB.

Figure 8A shows the specific-heat and δ-phase shift data for the axial configuration as a function of temperature, around the N-to-I phase transition. Again, the sharp change of δ-phase shift data was used to identify the excluded points of the coexistence N−I region (shaded area in Figure 8A). Equations 2a and 2b were used to get the fitting parameters, consigned in Table 2. All the parameter sets represent rather well the specific-heat data, as can be seen in Figure 8A as well as in the inset, where in a double logarithmic plot a linear relationship, with slope $-\alpha$, is shown between ΔC_p and reduced temperatures for both the nematic and isotropic wings. In this axial case with respect to the bulk, the coexistence region not only is larger but also is more asymmetric as is clearly shown in the inset of Figure 8A. On the whole, taking into account the critical exponent ($\alpha = 0.5$), amplitude ratio ($A_N/A_I = 3.17$), and the difference between T^{**} and T^* ($T^{**} - T^* \approx 0.02$ K), the axial case seems to exhibit a tricritical behavior similar to that in the bulk, pointing out that the axial confinement does not distort
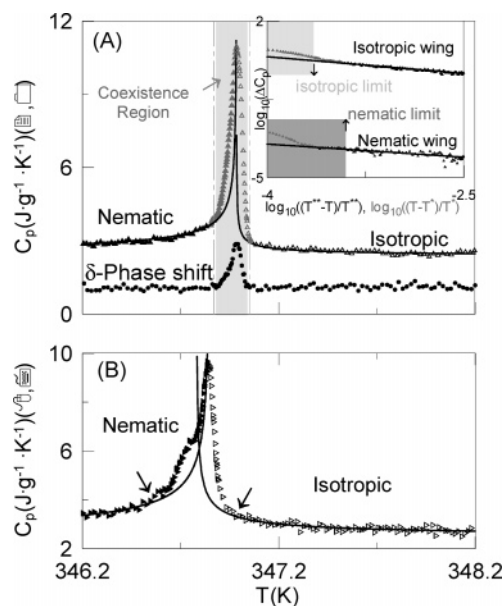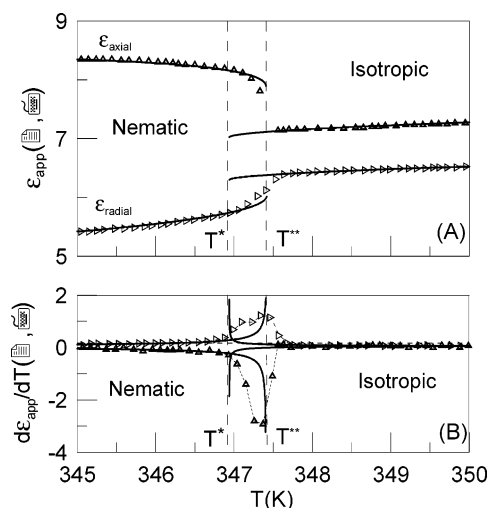

Figure 8. Specific heat for axially confined (A) and radially confined (B) 7OCB against temperature near the N-to-I transition. δ phase shift data ($\bullet$) in the axial case are included to delimit the coexistence region (shaded area), whereas the arrows point out the limits of the fittings in the radial case. The inset shows in a double logarithmic plot ΔC_p ($C_p - C_{p,background}$) vs reduced temperatures.

noticeably the bulk tricritical behavior. Only a depression of about 0.3 K in the set of characteristic temperatures (T_{NI}, T^{**}, and T^*, see Tables 1 and 2) as well as a slight diminution of the latent heat (ΔH_{NI}, see Table 1) and amplitude ratio (see Table 2) can be reported. It is important to realize that the depression in T_{NI} is smaller than that found by Iannacchione et al.[18,19] for other similar compounds (5CB, 7CB, and 8CB).

As for the radial confinement, the differences with respect to the bulk and axial cases are evident from Figure 2. First of all, δ-phase shift data cannot be used to determine the coexistence region if it exists. In fact, if only the δ-phase shift data around the transition are taken into account, the transition would be second order. Iannacchione et al.[19] measured the δ-phase shift (with an ac calorimeter) in the homologous 7CB radially confined to 200 nm Anopore membranes. Their δ-phase shift measurements showed a dip at the N-to-I transition also compatible with a lack of latent heat in the transition. Nevertheless, they attributed this behavior to a strong influence of elastic distortions that presumably would induce changes in the thermal diffusivity within the pores. Even so, the critical behavior of 7OCB radially confined through eq 2 was investigated, although is handicapped by the lack of information about the excluded points of the coexistence region. Likewise, the calculated latent heat ΔH_{NI} consigned in Table 1 is also strongly conditioned to this lack of information. In Figure 8B, the best fitting curves according to eq 2 are given. The coexistence region limits (marked by the arrows in Figure 8B) were approximately established by means of a trial and error procedure as a compromise between the physical meaning of the set-parameter fitting and the best mathematical accord with experimental points. Even so, the χ^2 (see Table 2) is an order of magnitude larger than in the case of the axial confinement and/or bulk fit results. In addition, the T^* value had to be held fixed in order to fit a comparable critical exponent α in both the nematic and isotropic wings. As a consequence, all the specific-heat fit results corresponding to the radial confinement, gathered in Table 2, as well as the ΔH_{NI} value consigned in Table 1, must be considered with extreme caution.

Heptyloxycyanobiphenyl Confinement in Cylindrical Pores

*J. Phys. Chem. B, Vol. 109, No. 49, 2005* **23215**

Figure 9. Apparent static dielectric permittivity data for the axial (up triangles) as well as for the radial (tilted triangles) alignments near the N-to-I phase transition (A) and its numerical derivative (B). Solid lines are fittings through eqs 3a, 6a, and 6b.


Figure 10. The calculated average order parameters (bulk, circles; axial, vertical triangles; radial, horizontal triangles) from specific-heat data against $(T - T_{NI})$. The inset shows in more detail both the bulk and axial average order parameters in a 7 K temperature range.

Regarding the dielectric data of both axial and radial alignments, the analysis has been performed following a similar procedure to what it has been exposed in the previous section devoted to the bulk 7OCB. The isotropic permittivity data can be fitted by eq 3a, but mean permittivity data corresponding to both confined cases are not available. Nevertheless, similar fluidlike relations to eq 3b to account for the apparent permittivity data, ϵ_{axial} and ϵ_{radial}, could be proposed

$$\epsilon_{axial} = \epsilon_{axial}** + a_{axial}|T - T_{axial}**| +$$
$$A_{axial}{}^D|T - T_{axial}**|^{1-\alpha} \quad (6a)$$

$$\epsilon_{radial} = \epsilon_{radial}** + a_{radial}|T - T_{radial}**| +$$
$$A_{radial}{}^D|T - T_{radial}**|^{1-\alpha} \quad (6b)$$

in which the different parameters have a similar meaning to that which is given in eq 3a. The solid curves representative of the fitting results according to eqs 6 and 3a are shown in Figure 5, for the whole temperature range and also in Figure 9A, for a 5 K zoom around the N-to-I transition. Some parameter fits (α, the amplitudes ratio, and the temperatures $T*$ and $T**$) are also gathered in Table 2 along with the corresponding values of χ^2. First of all, it is important to remark that eqs 6 reproduce quite well the axial and radial apparent permittivity results for the whole temperature range as can be clearly observed from the extremely low values of χ^2. Likewise, despite the independent way in which the fittings have been performed, a similar α value is obtained (0.54), virtually 0.5, if we take into account the limit of experimental error and, surprisingly, the same value for $T**$ ($\approx$347.4 K). Both sets of isotropic apparent permittivity data (axial and radial configurations in the I phase) are more or less parallel one to another (see Figure 9A), resulting in the same fitting parameters with the obvious exception of $\epsilon*$ (see eq 3a). The critical amplitudes ratio, that is to say, ($A_{axial}{}^D/A_{I,axial}{}^D$) and ($A_{radial}{}^D/A_{I,radial}{}^D$) are 3.58 and −3.68, respectively, being comparable between them (in absolute value) and also comparable to the amplitude ratio of the axial specific-heat data and, to a lesser extent, to the radial specific-heat data. The numerical derivative of experimental data shown in Figure 9A are presented in Figure 9B. Although the axial derivative data are negative, its absolute value mimics the specific-heat-like anomaly shown in Figure 8A. What it is surprising is that
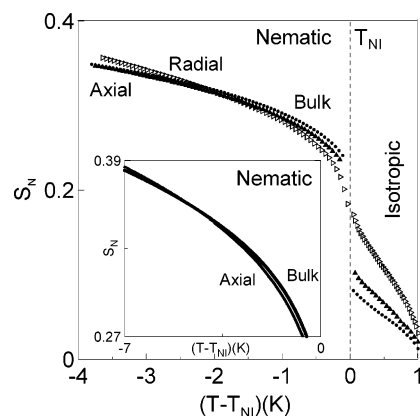
the radial derivative data presented in Figure 9B not only mimics the radial specific-heat anomaly as a whole but also presents a shoulder, pointing out that irrespective the experimental technique used, the shoulder is inherent to the radial confinement. The question now is addressed to what kind of phenomenon could this shoulder represent? Regardless of whether the true reply can be inferred from the present information, the possibility of nematic prewetting does not seem reasonable because the shoulder should be shifted to higher temperatures than T_{NI}.[20]

4.3. Overall Discussion. It is well-known that surface effects play the role of an external field that tries to drive the first-order N-to-I transition to a second order in nature.[53] Nevertheless, it seems doubtless from specific-heat data as well as dielectric measurements that bulk 7OCB and confined 7OCB in axial configuration display a comparable tricritical behavior at the N-to-I transition. This fact is additionally supported by the calculated average order parameter, using eq 4, for both the bulk and axial confinement specific-heat data as shown in Figure 10 and also in the inset of this figure.

What it is not so clear is what happens to confined 7OCB in radial configuration. The specific-heat data analysis is handicapped by the absence of experimental data about the limits of the coexistence region, the existence of which being an irrefutable signature of its first-order character. Likewise, the absence of thermal hysteresis from specific-heat data (Figure 3) along with the existence of a relevant thermal hysteresis (about 1 K) from dielectric measurements (inset of Figure 5) should stand out. In addition, this thermal hysteresis is comparable to what is exhibited in axial configuration, as can be seen in the inset of Figure 5.

Now, let us consider the overall effects responsible of shifting, suppression, and rounding of the N-to-I phase transition in confined cylindrical geometries. Basically, the surface anchoring and finite size effects should be considered as it was proposed in the past.[18,19,54−58] From the Landau−de Gennes theory of liquid crystals, the N-to-I transition temperature increases if the surface aligns the liquid crystal molecules to form a boundary layer which is more ordered than the bulk (surface-induced nematic order), being the calculated shift in the transition temperature at most 0.5 K[55,56] upward. The specific-heat suppression at the transition is basically due to the molecules of this boundary layer that do not contribute to the phase transition. This fact should be very well evidenced from dielectric measurements as a reduction of the static permittivity. Nevertheless, the elastic distortions have the opposite effect on the transition temperature, being the shift in temperature about
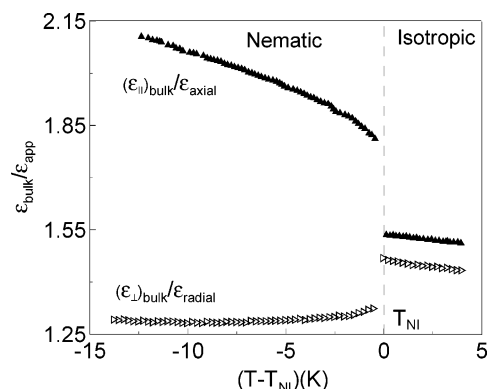
Figure 11. The ratio of the static permittivity bulk data over apparent static permittivity data for axial (vertical triangles) as well as (horizontal triangles) radial alignments against $(T - T_{NI})$.

1 K[14,18,19,57] downward. The finite size effects on first-order phase transitions in general, and on the N-to-I transition in particular[57,58] are less important. Even so, the N-to-I transition tends to shift downward. In addition, small finite clusters would undergo isotropy at lower temperatures than those in bulk. If they are poorly correlated, the liquid crystal undergoes the phase transition separately leading to a rounding of specific-heat peak and a global reduction in the N-to-I transition temperature.

The shifting, suppression, and rounding of the N-to-I transition in confined 7OCB lead to comparable specific-heat results in relation to other homologous compounds in cylindrical geometry investigated by other researchers.[18−20,57] More recently dynamic dielectric results on cylindrical confinement[27,28,59] are reported although in a much lesser extent if only static dielectric results are taken into account.[27] As for our static dielectric results, strangely no appreciable shifting in temperatures can be reported neither between both confined configurations nor between bulk and these confined cases (see inset of Figure 5). The very recent static dielectric measurements of Leys et al.[27] on the SmA-to-I transition of decylcyanobiphenyl (10CB) under cylindrical confinement in treated and untreated Anopore membranes lead to a higher transition temperature for the treated membrane and lower transition temperature for the untreated membrane as compared to the bulk.

Let us now consider the evolution of the apparent static permittivity (ϵ_{app}) in both confined cases. Results make it evident that the apparent static permittivity values on the isotropic phase mainly account for the response of the molecular reorientations around molecular short axis giving rise to lower values when the molecular reorientations are more hindered. In fact the difference, on the isotropic phase, of the two sets of ϵ_{app} data gives information on the different magnitude of the molecular pinning, stronger for the radial case than for the axial case as could be expected from the calculated average order parameter (Figure 10). Likewise, their trend to increase ϵ_{app} when temperature does, unlike bulk data, would point out that as the molecules gain more thermal energy, more molecules in the surface-induced nematic shell contribute to the value of ϵ_{app}.

If we take into account the nematic phase of the axial case, the value of ϵ_{app} has a comparable meaning as in the isotropic phase. So, the molecules that would not contribute due the surface-induced nematic shell could be estimated at more or less 40% near the T_{NI}, a value not too different from that obtained from the axial specific heat peak suppression (34%). In addition, at lower temperatures, the trend of ϵ_{axial} as temperature decreases is fully different in relation to the $\epsilon_{\parallel}$ of the bulk; see Figures 4 and 5 as well as Figure 11. In this figure, the ratio $(\epsilon_{\parallel})_{Bulk}$ over ϵ_{axial} is shown for comparison purposes.

The continuous increasing of this ratio as temperature decreases is a result of the fact that in the bulk more molecules contribute to the dielectric constant than in the axial case. This behavior could be explained as a consequence of the surface pinning effect that increases the number of molecules in the boundary layer (at low temperatures the molecules have less thermal energy to be disordered) in such a way that the lower the temperature, the fewer molecules contribute.

As for the nematic phase of the radial case, the physical meaning of its apparent dielectric permittivity values has to be compared to $(\epsilon_\perp)_{Bulk}$. In the later, the permittivity values mainly account for the precession of the molecular long-axis around the nematic director and for the rotation of the molecules around the long axis.[60] If we assume that ϵ_{radial} values account for the same kind of molecular motions as $(\epsilon_\perp)_{Bulk}$, the surface pinning of the molecules, even if this is strong, should affect to a lesser degree the static dielectric permittivity near the T_{NI} because these movements are sterically less hindered than the molecular reorientations around the short molecular axis. Nevertheless, the trend of ϵ_{radial} with respect to $(\epsilon_\perp)_{Bulk}$, that is to say, the ratio of $(\epsilon_\perp)_{Bulk}$ over ϵ_{radial}, tends to increase at low enough temperatures as temperature decreases (see Figure 11), again in such a way that the lower the temperature, the fewer molecules that contribute. Obviously, this effect is in a lesser degree than in the axial case, as has been already reasoned.

Finally, in Figure 10, the three computed average order parameters (bulk as well as the two confined configurations) extracted from specific-heat data through eq 4 are shown. It is important to realize that in the computed radial case, no coexistence region has been excluded. Although the absolute values are approximate, the trends and relative values can be compared. So, in the isotropic phase the existence of a nematic-induced order can be clearly observed for the axial and radial cases as a consequence of the pinning of the molecules at the surface, stronger for the radial than for the axial case. On the nematic side, although the evolution of the order parameters against temperature for bulk and axial configurations are very close, at low temperatures both curves cross each other as can be observed in the inset of Figure 10. As for the radial order parameter this fact is clearer than for the axial case. Both trends shown in Figure 10 reinforce the interpretation of dielectric data.

5. Concluding Remarks

Specific heat as well as static dielectric measurements on 7OCB, in bulk and cylindrically confined to 200 nm Anopore, are presented.

The N-to-I phase transition has been analyzed from the two measurements comparing bulk and confined axial and radial cases. The consistency of all data has been fully discussed. Qualitatively, the confined specific-heat results for 7OCB were comparable with those reported in the literature[18,19] for its homologous 7CB. However, the specific-heat peak depression in temperature of both confined cases from that of the bulk 7OCB is smaller than that reported for its homologous 7CB.[19] As for latent heat, in 7OCB, a diminution of about 12% has been observed between the bulk and both the axial and radial confinements. Nevertheless, in the homologous 7CB, the latent heat increases when the axial confinement is compared with the bulk, whereas it decreases almost 20% when radial confinement is considered.[19] As for dielectric results, taking into account the lack of such information in the literature, the comparison with those published[31] was exclusively restricted to bulk 7OCB. The apparent static dielectric data of the confined 7OCB have been analyzed for the first time, as far as we know, by means of the fluidlike model, giving rise to a quite good agreement.

Heptyloxycyanobiphenyl Confinement in Cylindrical Pores

J. Phys. Chem. B, Vol. 109, No. 49, 2005 **23217**

Both types of measurements (specific heat and static dielectric permittivity) lead to a comparable tricritical behavior for the N-to-I phase transition in bulk 7OCB and also certify a similar tricritical behavior for axial confinement, pointing out that this kind of confinement does not distort noticeably the bulk tricritical behavior. Contrarily, for radial confinement, both kinds of measurements seem to display a non-well-defined behavior for the N-to-I phase transition, likely due to elastic distortions.

A simple empirical method based on a simplified Landau−de Gennes free energy expansion has been used to get the temperature dependence of the average orientational order parameter from the specific-heat data. For the bulk, the trend of the model calculated order parameter is in a good agreement with direct dielectric anisotropy measurements, making it possible to obtain, following the same model, the calculated order parameters for the confined cases. Its comparative analysis allows us to reproduce most of the observed features from other experimental techniques (static dielectric data) as well as those reported in the literature. So, the static dielectric data in nematic as well as in isotropic phases account for the existence of a surface-induced nematic order layer in both confined cases (axial and radial). In a similar way, the computed average order parameter accounts for the existence of this surface-induced nematic order and, also, for a disordering effect caused by the pore surface in the nematic phase near the N-to-I transition, stronger for the radial case than for the axial case (close to the transition, the radial order parameter is lower than the axial and bulk order parameters). This effect was already found by Iannacchione et al.,[19] in a similar study on cylindrically confined pentylcyanobiphenyl (5CB). What is really different in our study as for the case of 5CB[19] is that at low enough temperatures the radial-order parameter is higher than the others (axial- and bulk-order parameters). The most probable explanation to this fact is suggested as follows: When temperature decreases, the surface-induced nematic order layer increases as a result of a combination between the thermal energy loss of the molecules and the surface anchoring energy (greater in the radial case than in the axial one[18]) giving rise to an overall increasing of the average order parameter, greater for the radial case than for the axial case.

References and Notes

(1) Doane, J. W. *Liquid Crystals*: *Their applications and Uses*; Bahadur, B., Ed.; World Scientific: Hackensack, NJ, 1990.

(2) *Liquid Crystals in Complex Geometries formed by Polymer and Porous Networks*; Crawford, G. P., Zumer, S., Eds.; Taylor and Francis: London, 1996.

(3) Lin, H.; Palffy-Muhoray, P.; Lee, M. A. *Mol. Cryst. Liq. Cryst.* **1991**, *202*, 189.

(4) Busch, K.; John, S. *Phys. Rev. Lett.* **1999**, *83*, 967.

(5) Yablonovitch, E. *Nature* **1999**, *401*, 539.

(6) Leonard, S. W.; Mondia, J. P.; van Driel, H. M.; Toader, O.; John, S.; Busch, K.; Birner, A.; Gösele, U. *Phys. Rev. B* **2000**, *61*, R2389.

(7) Wiersma, D. S.; Colocci, M.; Righini, R.; Aliev, F. *Phys. Rev. B* **2001**, *64*, 144208.

(8) Wiersma, D. S.; Cavalieri, S. *Phys. Rev. E* **2002**, *66*, 056612.

(9) Wiersma, D. S.; Lagendijk, A. *Phys. Rev. E* **1996**, *54*, 4256.

(10) Lawandy, N. M.; Balachandran, R. M.; Gomes, A. S. L. Sauvin E. *Nature* **1994**, *368*, 436.

(11) Anopore inorganic membranes is commonly used for laboratory filtration applications. More information can be obtained in www.whatman.com.

(12) Crawford, G. P.; Steele, L. M.; Ondris-Crawford, R.; Iannacchione, G. S.; Yeager, C. J.; Doane, J. W.,; Finotello, D. *J. Chem. Phys.* **1992**, *96*, 7788.

(13) Iannacchione, G. S. *Fluid Phase Equilib.* **2004**, *222*, 177.

(14) Bellini, T.; Clark, N. A.; Muzny, C. D.; Wu, L.; Garland, C. W.; Shaefer, D. W.; Oliver, B. *J. Phys. Rev. Lett.* **1992**, *69*, 788.

(15) Wu, L.; Zhou, B.; Garland, C. W.; Bellini, T.; Shaefer, D. W. *Phys. Rev. E* **1995**, *51*, 2157.

(16) Quian, S.; Iannacchione, G. S.; Finotello, D. *Phys. Rev. E* **1996**, *53*, R4291.

(17) Bellini, T.; Buscaglia, M.; Chiccoli, C.; Mantegazza, F.; Pasini, P.; Zannoni, C. *Phys. Rev. Lett.* **2000**, *85*, 1008.

(18) Iannacchione, G. S.; Finotello, D. *Phys. Rev. Lett.* **1992**, *69*, 2094.

(19) Iannacchione, G. S.; Finotello, D. *Phys. Rev. E* **1994**, *50* (6), 4780.

(20) Liu, X.; Allender, D. W.; Finotello, D. *Europhys. Lett.* **2002**, *59*, 848.

(21) Iannacchione, G. S.; Mang, J. T.; Kumar, S.; Finotello, D. *Phys. Rev. Lett.* **1994**, *73*, 2708.

(22) Crawford, G. P.; Ondris-Crawford, R.; Zumer, S.; Doane, J. W. *Phys. Rev. Lett.* **1993**, *70*, 1838.

(23) Zalar, B.; Zumer, S.; Finotello, D. *Phys. Rev. Lett.* **2000**, *84*, 4866.

(24) Zalar, B.; Blinc, R.; Zumer, S.; Jin, T.; Finotello, D. *Phys. Rev. E* **2002**, *65*, 041703.

(25) Aliev, F. M.; Breganov, M. N. *Sov. Phys. JETP* **1989**, *68*, 70.

(26) Aliev, F. M.; Nazario, Z.; Sinha, G. P. *J. Non-Cryst. Solids* **2002**, *305*, 218.

(27) Leys, J.; Sinha, G.; Glorieux, C.; Thoen, J. *Phys. Rev. E* **2005**, *71*, 051709.

(28) Diez, S.; de la Fuente, M. R.; Pérez-Jubindo, M. A.; López, D. O.; Salud, J.; Tamarit, J. Ll. Submitted for publication in *Phys. Rev. E*.

(29) Jin, T.; Zalar, B.; Lebar, A.; Vilfan, M.; Zumer, S.; Finotello, D. *Eur. Phys. J. E* **2005**, *16*, 159.

(30) Landau, L. D.; Lifshitz, E. M. *Statistical Physics*; Pergamon: Oxford, 1968.

(31) Rzoska, S. J.; Ziolo, J.; Sulkowski, W.; Jadzyn, J.; Czechowski, G. *Phys. Rev. E* **2001**, *64*, 052701.

(32) Lafouresse, M. C.; Sied, M. B.; Allouchi, H.; López, D. O.; Salud, J.; Tamarit, J. Ll. *Chem. Phys. Lett.* **2003**, *376*, 188.

(33) Sied, M. B.; Salud, J.; López, D. O.; Barrio, M.; Tamarit, J. Ll *Phys. Chem. Chem. Phys.* **2002**, *4*, 2587.

(34) Puertas, R.; Rute, M. A.; Salud, J.; López, D. O.; Diez, S.; van Miltenburg, J. C.; Pardo, L. C.; Tamarit, J. Ll.; Barrio, M.; Pérez-Jubindo, M. A.; de la Fuente, M. R. *Phys. Rev. B* **2004**, *69*, 224202.

(35) Crawford, G. P.; Stannarius, R.; Doane, J. W. *Phys. Rev. A* **1991**, *44*, 2558.

(36) Crawford, G. P.; Allender D. W.; Doane, J. W. *Phys. Rev. A* **1992**, *45*, 8693.

(37) Kralij, S.; Zumer, S. *Phys. Rev. E* **1995**, *51*, 366.

(38) Ziherl, P.; Zumer, S. *Phys. Rev. E* **1996**, *54*, 1592.

(39) Bradac, Z.; Kralij, S.; Zumer, S. *Phys. Rev. E* **1998**, *58*, 7447.

(40) Marroum, R. M.; Iannacchione, G. S.; Finotello, D.; Lee, M. A. *Phys. Rev. E* **1995**, *51*(6), R2743.

(41) Sied, M. B.; Salud, J.; López, D. O.; Allouchi, H.; Diez, S.; Tamarit, J. Ll. *J. Phys. Chem. B* **2003**, *107*, 7820.

(42) Anisimov, M. A. *Critical Phenomena in Liquids and Liquid Crystals*; Gordon and Breach Science Publishers: Amsterdam, 1991.

(43) Keyes, P. H.; Shane, J. R. *Phys. Rev. Lett.* **1979**, *42*, 722.

(44) Mukherjee, P. K. *Phys. Rev. E* **1995**, *51*, 4570.

(45) Drozd-Rzoska, A.; Rzoska, S. J.; Ziolo, J.; Jadzyn, J. *Phys. Rev. E* **2001**, *63*, 052701.

(46) Mistura, L. *J. Chem. Phys.* **1973**, *59*, 4563.

(47) Islander, S. T. Zimmermann, W., Jr. *Phys. Rev. A* **1973**, *7*, 188.

(48) Huster, M. E.; Stine, K. J.; Garland, C. W. *Phys. Rev. A* **1987**, *36*, 2364.

(49) Stine, K. J.; Garland, C. W. *Phys. Rev. A* **1989**, *39*, 3148.

(50) Sied, M. B.; López, D. O.; Tamarit, J. Ll.; Barrio, M. *Liq. Cryst.* **2002**, *29*, 57.

(51) Kasting, G. B.; Lushington, K. J.; Garland, C. W. *Phys. Rev. B* **1980**, *22*, 321.

(52) Keyes, P. H. *Phys. Lett. A* **1978**, *67*, 132.

(53) Mukhopadhyay, R.; Yethiraj, A.; Bechhoefer, J. *Phys. Rev. Lett.* **1999**, *83*, 4796.

(54) de Gennes, P. G. *The Physics of Liquid Crystals*; Oxford University Press: Oxford, 1974.

(55) Sheng, P. *Phys. Rev. Lett.* **1976**, *37*, 1059.

(56) Sheng, P. *Phys. Rev. A* **1982**, *26*, 1610.

(57) Kuzma, M.; Labes, M. M. *Mol. Cryst. Liq. Cryst.* **1983**, *100*, 103.

(58) Golemme, A.; Zumer, S.; Allender, D. W.; Doane, J. W. *Phys. Rev. Lett.* **1988**, *61*, 2937.

(59) Ryabov, Y. E.; Puzenko, A.; Feldman, Y. *Phys. Rev. B* **2004**, *69*, 014204.

(60) de Jeu, W. H. *Physical Properties of Liquid Crystalline Materials*; Gordon and Breach Science Publishers, Inc.: London, 1980.